DFT+DMFT study of dopant effects in the heavy-fermion compound $CeCoIn_5$

Hong Chul Choi [1,2,*] Eric D. Bauer,[3] Filip Ronning,[4] and Jian-Xin Zhu [1,5,†]

[1]*Theoretical Division, Los Alamos National Laboratory, Los Alamos, New Mexico 87545, USA*
[2]*Center for Correlated Electron Systems, Institute for Basic Science (IBS), Seoul 08826, Korea*
[3]*Materials Physics and Application Division, Los Alamos National Laboratory, Los Alamos, New Mexico 87545, USA*
[4]*Institute for Materials Science, Los Alamos National Laboratory, Los Alamos, New Mexico 87545, USA*
[5]*Center for Integrated Nanotechnologies, Los Alamos National Laboratory, Los Alamos, New Mexico 87545, USA*

(Received 25 August 2021; revised 27 January 2022; accepted 7 March 2022; published 16 March 2022)

We study the dopant-induced inhomogeneity effect on the electronic properties of heavy fermion $CeCoIn_5$ using a combined approach of density functional theory (DFT) and dynamical mean-field theory (DMFT). The inhomogeneity of the hybridization between Ce-4f and conduction electrons is introduced to impose the inequivalent Ce atoms with respect to the dopant. From the DFT to the DFT+DMFT results, we demonstrate a variation of the hybridization strength depending on the hole or electron doping. A drastic asymmetric mass renormalization could be reproduced in the DFT+DMFT calculation. Finally, the calculated Kondo temperature reflects the different development of the heavy quasiparticle states, depending on the dopant.

DOI: 10.1103/PhysRevB.105.115121

I. INTRODUCTION

Heavy-fermion systems (HFSs) [1–3] have shown unconventional superconductivity, Kondo effect, valence fluctuations, magnetism, and exotic coexisting phases. The renormalized quasiparticle kinetic energies observed in the heavy fermion originate from the Kondo effect. The strength of the Kondo effect is determined by the hybridization function (Δ) between localized and conduction electrons, and the density of state (N_F) at the Fermi level (E_F). Strong hybridization could suppress the renormalization effect over the competition with the Coulomb interaction. The wave function of the 4f electrons is deeply distributed inside the atomic radius close to the atomic wave function. However, the energy gain through the Kondo effect could drive a crossover from a localized moment into a highly renormalized itinerant quasiparticle state near E_F. In addition, the atomic multiplet of Ce-4f valence states provides an additional incoherent feature, being identified as lower and upper Hubbard bands. The three-peak spectral function $A(k, \omega)$ represents the characteristic dual nature of the strongly correlated f-electron system.

The Ce-based heavy-fermion compounds are one prototypical family of HFSs. $CeIn_3$ shows an antiferromagnetic ground state with $T_N = 10$ K, where superconductivity with $T_c = 0.21$ K emerges under a critical pressure of 2.6 GPa [4,5]. $CeMIn_5$ (M=Co, Rh, Ir) [6–8] is synthesized by inserting MIn_2 layers between $CeIn_3$ layers. In these compounds, $CeCoIn_5$ and $CeIrIn_5$ are unconventional superconductors at $T_c = 2.3$ and 0.4 K, respectively, indicative of Ce-4f electrons being delocalized, whereas $CeRhIn_5$ is an antiferromagnet ($T_N = 3.8$ K) with localized 4f electrons at ambient pressure. The substitution of Cd [9–16], Ru [17], or Hg [13,14] (hole doping) and Sn [12–15,18–21], Zn [22,23], or Pt [14] (electron doping) has been reported to either promote antiferromagnetic (AFM) or metallic phases. In comparison to In ($4d^{10}5p^1$), Cd and Sn have the valence states of $4d^{10}$ and $4d^{10}5p^2$, respectively. The one less (more) electron would be expected to reduce (enhance) the hybridization. Experimentally, angle-resolved photoemission spectroscopy has indeed demonstrated the suppression of the band hybridization in Cd-doped $CeCoIn_5$ [16]. The electron or hole doping affects the ground state of $CeCoIn_5$ asymmetrically. Only one-percent Cd substitution causes the AFM ground state with a local moment on the Ce sites ($\sim$0.7 μ_B/Ce), while the Sn substitution leads to a complete disappearance of superconductivity for a critical concentration $\sim\sim$ 3.6% Sn. In addition, the extended x-ray absorption fine-structure measurements have suggested the preference of dopant atoms to the Ce-In plane [13,21], which means an inhomogeneous distribution of dopants.

Density functional theory (DFT) has proven to be very effective in helping to unravel the effects of doping in the 115s. For example, DFT could help identify various local atomic environments observed by nuclear magnetic resonance (NMR) [12,24]. DFT calculations also helped to uncover the local increase (decrease) in the hybridization caused by Sn (Cd) dopants [14]. Furthermore, the open-core (setting 4f states inside the core state) or the conventional (setting 4f states as valence states) DFT provides a hint of whether 4f states might be localized or delocalized. [12] Therefore, DFT proved itself as a powerful tool to incorporate material-specific information, that is, the structure and atomic configuration of the real compound. On the other hand, it is known to underestimate the effect of electronic correlations in heavy-fermion systems. This inadequacy can be remedied by dynamical mean-field theory (DMFT), which has successfully captured the correlation-induced crossover between

*chhchl@gmail.com
†jxzhu@lanl.gov

localization and delocalization in strongly correlated systems. Via a strong band renormalization, the correlation effect on the electronic structure and optical properties were well reproduced by DFT+DMFT calculations [25–27]. Using the virtual crystal approximation, a DFT+DMFT study reproduced the general trends of the doping effect [28]. However, the impact of the dopant-induced inhomogeneity in real compounds has not been addressed.

Here we revisit the effect of doping on $CeCoIn_5$ to take into account the inhomogeneity with respect to the distance from a dopant to a Ce atom. We break the equivalence of Ce atoms by placing the dopant close to a specific Ce atom. The electronic structure is investigated by DFT and DFT+DMFT calculations. The DFT results give a hint about the different behavior of hole versus electron substitutions, while its limitation is also shown. The small change in the hybridization in the DFT quasiparticle could turn into a totally different phase through the DMFT impurity solver. The inhomogeneity of the self-energy and the hybridization functions is shown in the DFT+DMFT results. The different evolution of the heavy quasiparticle band induced by the dopant will be discussed with the calculated Kondo temperature.

The paper is organized as follows: Section II explains the computational method. In Sec. III, we address calculated crystal structures, and the DFT and DFT+DMFT results. Also, the calculated Kondo temperature will be provided here. Section IV presents a summary and concluding remarks.

II. COMPUTATIONAL DETAILS

The charge self-consistent version of DFT+DMFT [29], as implemented in Ref. [30], is based on the full-potential linearized augmented plane-wave (FP-LAPW) band method [31]. To solve the impurity problem, we used the vertex-corrected one-crossing approximation (OCA) [29,32–34], where the DMFT local self-energy $\Sigma(\omega)$ is calculated on the real frequency ω. The correlated $4f$ electrons are treated dynamically by $\Sigma(\omega)$, while all other delocalized *spd* electrons are treated on the DFT level. The charge and spin fluctuations considered in DMFT enable the correct description of the Kondo effect. $\Sigma(\omega)$ is calculated from the corresponding impurity problem, in which the Slater Coulomb integral parts for f electrons are taken into account ($F^0 = 5.0$ eV, $F^2 = 8.106\,936\,416\,18$ eV, $F^4 = 5.415\,433\,526\,01$ eV, and $F^6 = 4.004\,826\,589\,6$) [35]. A temperature of 5 meV is used in the calculations. To solve the impurity problem, we used the one-crossing approximation of the local self-energies [29]. RK_{max} of 7.0 and a 3000 k-point mesh are used throughout the calculation. The spin-orbit coupling is always included in the calculations. The total charge density and the self-energy through the DFT+DMFT iterations are converged within 10^{-5} and 10^{-4}, respectively.

The single-site DMFT solvers for the $4f$ state in each unique Ce cite are treated separately. The $4f$ state for the unique Ce sites will be denoted as Ce1 or Ce2. The intersite correlation beyond the single-site DMFT solver is included through the hybridization function (Δ). The local Green's function ($G_{loc} = \frac{1}{\omega - \epsilon_{\rm imp} - \Sigma - \Delta}$, with $\epsilon_{\rm imp}$ the impurity energy level, Σ the self-energy, and Δ the hybridization function between impurity and bath) and the lattice Green's function, computed by the DFT eigenvalue ($H_{\mathbf{k}}^{\rm DFT}$) and E_F, are self-consistently determined with the identical Σ. The projection operator ($P_{i,\mathbf{k}}$) is required to determine an impurity state from eigenstates in the lattice. In this study, we only use the jj basis to ignore the effect of the crystalline electric field (CEF) on $4f$ states. A CEF-driven ground state indeed emerges at lower temperature than 50 K in the family of $CeCoIn_5$ [36]. Practically, the impurity energy levels are well defined to have only intraorbital (diagonal) components by neglecting the interorbital components. Thus the impurity levels have only $j = 5/2$ and $j = 7/2$ states in each Ce atom. After the self-energy is computed in the impurity solver, the embedding operator ($E_{i,\mathbf{k}}$), where i is Ce1 or Ce2, and $\mathbf{k}$ is the crystal momentum, restores the contribution of the self-energy to each eigenstate in the lattice, regarding the distribution of the f orbital over momentum and energy. Using $\hat{P}_{1,\mathbf{k}}$, $\hat{P}_{2,\mathbf{k}}$, $\hat{E}_{1,\mathbf{k}}$, and $\hat{E}_{2,\mathbf{k}}$, where 1 is the Ce1-$4f$ states, 2 is the Ce2-$4f$ states, and $\mathbf{k}$ is the momentum, the self-consistent equations are defined as follows:

$$\frac{1}{\omega - \epsilon_{1,\rm imp} - \Sigma_i - \Delta_i} = \sum_{\mathbf{k}} \hat{P}_{i,\mathbf{k}}\left[\left(\omega + E_F - H_{\mathbf{k}}^{\rm DFT} - \hat{E}_{i,\mathbf{k}}\Sigma_i\right)^{-1}\right]. \quad (1)$$

Here, $\epsilon_{i,\rm imp}$, Σ_i, and Δ_i mean the impurity energy level, self-energy, and hybridization function, respectively. The index i represents the different impurities Ce1 or Ce2. The long-range correlation effect is taken into account through Δ_i. It is noteworthy that the imaginary parts of Σ_i and Δ_i have negative values to ensure the causality of a retarded Green's function.

III. NUMERICAL RESULTS

Figure 1(a) presents the supercell structure of $CeCoIn_5$ made from the original primitive unit cell as shown in Fig. 1(c). We adopt the minimum size of the $1 \times 1 \times 2$ supercell of $CeCoIn_5$, which has two Ce, two Co, and 10 In atoms for our calculations. Ce(1) at (0,0,0) and Ce(2) at (0,0,0.5) are equivalent in the pristine structure. In the primitive cell, In atoms are distinguished as those [In(1)] in the Ce plane and the other four In atoms [In(2)] in between the Co plane and the Ce-In plane. For simplicity, we choose the dopant atom (Cd, Sn, or Hg) to occur at the In(1) position of the Ce(1) plane. This is consistent with the extended x-ray absorption fine-structure measurement, which indicates that these dopant atoms preferentially substitute on the In(1) site. These substitutions force Ce(1) and Ce(2) to become inequivalent. In this work, we examine the electronic structure of $CeCoIn_5$ (pristine), $CeCo(In_{0.9}Cd_{0.1})_5$ (Cd-doped $CeCoIn_5$), $CeCo(In_{0.9}Hg_{0.1})_5$ (Hg-doped $CeCoIn_5$), and $CeCo(In_{0.9}Sn_{0.1})_5$ (Sn-doped $CeCoIn_5$).

First we report the conventional DFT calculations of the doped $CeCoIn_5$. Figure 2 shows the density of states (DOS) of (a) Ce(1)-$4f$ states, (b) Ce(2)-$4f$ states, and (c) Co-$3d$ states. We note that the DOS for the two Co atoms are identical due to the inversion symmetry. Depending on the dopant, the Ce-$4f$ bands are shifted with respect to the pristine case (red line). The two peaks in Figs. 2(a) and 2(b) correspond to the $j = 5/2$ (left peak) and $j = 7/2$ (right peak) states split by

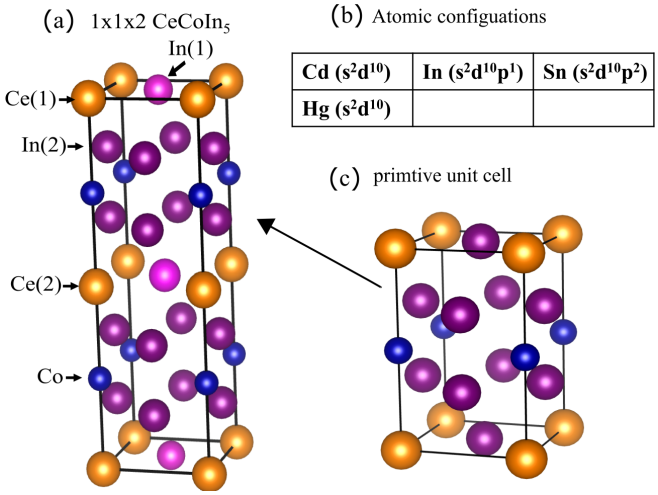

FIG. 1. (a) The schematic crystal structures [37] of the $1 \times 1 \times 2$ supercell of $CeCoIn_5$ The different colors represent the different atoms. Indium (In) atoms have the magenta (In1) and purple (In0) colors. For the doped case, the dopant atom replaces In1 to give the concentration of a 10%-doped structure. Additionally, the two types of Ce atoms are distinguished as Ce1 (close to the dopant) and Ce2 (away from the dopant). (b) The atomic configurations of Cd, In, Sn, and Hg are compared. (c) The primitive unit cell of $CeCoIn_5$ is provided.

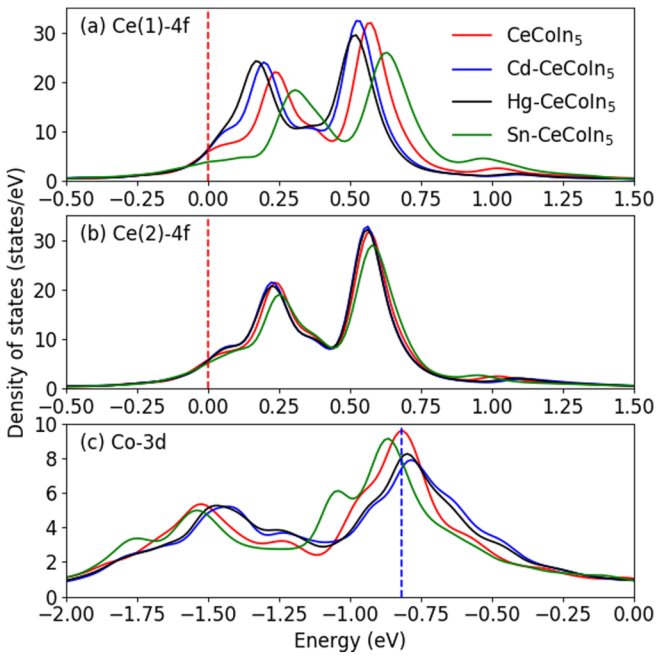

FIG. 2. The density of states for the (a) Ce1-4f, (b) Ce2-4f, and (c) Co-3d states calculated in four different structures with DFT. The labels represent $CeCoIn_5$ (pristine), $CeCo(In_{0.9}Cd_{0.1})_5$ (Cd-doped $CeCoIn_5$), $CeCo(In_{0.9}Hg_{0.1})_5$ (Hg-doped $CeCoIn_5$), and $CeCo(In_{0.9}Sn_{0.1})_5$ (Sn-doped $CeCoIn_5$). The red vertical line represents the Fermi level. The blue vertical line is provided as a guide to compare the shift of the bands with respect to the dopant.

TABLE I. Ce-4f electron occupancy in the DFT calculations.

n_f (electron/Ce atom)	Ce1	Ce2
$CeCoIn_5$	0.9704	0.9704
$CeCo(In_{0.9}Cd_{0.1})_5$	0.9475	0.9663
$CeCo(In_{0.9}Hg_{0.1})_5$	0.9561	0.9668
$CeCo(In_{0.9}Sn_{0.1})_5$	1.008	0.9738

spin-orbit coupling (∼0.3 eV). This value is inherited into the impurity solver in the DFT+DMFT calculation. Hereafter, we focus on the $j = 5/2$ states, which mainly contribute the states around E_F.

As Cd and Hg (Sn) have one less (more) electron than In [see Fig. 1(b)], the shift of the chemical potential with respect to Ce-4f states would be lowered (increased) in the Cd- and Hg-doped (Sn-doped) cases. The trend in Figs. 2(a) and 2(b) for Ce(1)-4f and Ce(2)-4f in the pristine and doped cases does not follow this simple intuition. In comparison to the $j = 5/2$ peak of the pristine Ce-4f states, the peak for the Cd- and Hg-doped (Sn-doped) cases is shifted toward (away from) the Fermi energy level. Also, the DOS at E_F are increased in Cd- and Hg-doped $CeCoIn_5$ systems, whereas that of the Sn-doped $CeCoIn_5$ is decreased. Those results indicate that the effect of doping on the 4f states is not clearly seen within the DFT method. On the other hand, the inhomogeneous feature between Ce(1) and Ce(2) sites could be identified. In addition, Table I shows that Ce-4f electron occupancy in the DFT calculation depends on whether it is hole doped or electron doped, the meaning of which will be discussed later.

We also explore the doping effects on the 3d bands of the transition-metal Co. As shown in Fig. 2(c), the band center of Co-3d states is shifted toward E_F in the Cd- and Hg-doped $CeCoIn_5$ cases, while that of the Sn-doped $CeCoIn_5$ is moved away from E_F. Such behavior is in agreement with a rigid band picture.

In the remainder of this paper, we will discuss how correlations influence the electron- and hole-doped cases. Through the DFT+DMFT calculations, Ce(1)-4f and Ce(2)-4f states are treated as correlated impurity states, denoted by Ce1 and Ce2. The DOS ($-\mathrm{Im}G_{loc}$) of Ce1 and Ce2 are provided in Fig. 3. In $CeCoIn_5$, the peak of $j = 5/2$ states grows as the temperature lowers. In comparison to Figs. 2(a) and 2(b), the width of the peaks is highly reduced and pushed towards E_F under the correlation effect as captured by the DMFT self-energy. The DOS at E_F of the Ce1 in the Sn-doped case is much larger than others in the Ce(1) site, where the dopant is located at the nearest-neighbor site, while that of the Ce2 in the Ce(2) site is slightly higher than others. On the other hand, the suppression of that in the Cd/Hg-doped case could be seen with respect to the pristine case. These characteristic features are not seen in Fig. 2 due to the much broader bandwidth of 4f states with the DFT calculations. The spin-orbit side band is attributed to the transition between $j = 5/2$ and $j = 7/2$ states [38]. The Sn dopant due to the increased hybridizations pushes the Ce1 away from the Kondo limit. The enhanced DOS of the Ce(1) is associated with its closer proximity to the Fermi liquid in $CeCo(In_{0.9}Sn_{0.1})_5$. We note that the OCA method could suffer a violation of Fermi-liquid behavior at

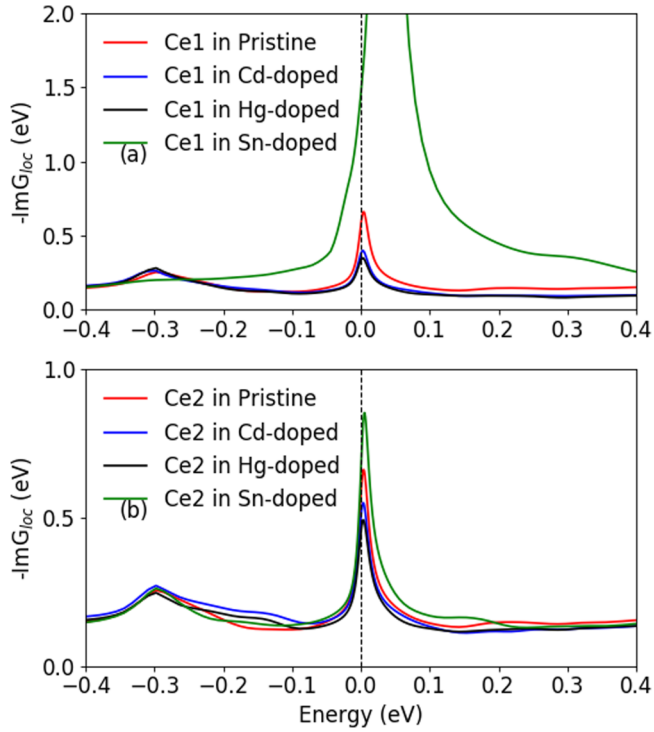

FIG. 3. The imaginary part of the local Green's functions for (a) Ce1 $j = 5/2$ states and (b) Ce2 $j = 5/2$ states in different structures with DFT+DMFT. The labels represent $CeCoIn_5$ (pristine), $CeCo(In_{0.9}Cd_{0.1})_5$, $CeCo(In_{0.9}Hg_{0.1})_5$, and $CeCo(In_{0.9}Sn_{0.1})_5$.

very low temperature for a one-channel Anderson impurity model [34]. In the Sn-doped case, when the Kondo coherence is strong, caution should be taken as to whether the feature of the OCA-derived spectral function accurately satisfies the Fermi-liquid behavior. In case of the hole-doped calculations (Cd or Hg), Ce(1) shows a reduction of the DOS relative to the pristine case. This opposition behavior is consistent with stabilizing a magnetic state upon hole doping.

We examine the $4f$ electron occupancy (n_f) for the pristine and doped cases. As summarized in Table II, the calculated n_f in the Sn-doped case is larger than the others. This trend looks contradictory to the intuitive view of valence change from $4f^1$ (Ce^{3+}) to f^0 (Ce^{4+}) under strong hybridization. Therefore, within a simple hybridization picture, one would expect that the hole (electron) doping would drive the valence of Ce states toward f^1 (f^0). Here we bring up a different insight: As shown in Fig. 4, although the total number of Ce-$4f$ electron occupation is larger in the Sn-doped case, under the electron doping, the probability of f^1 configuration decreases while

TABLE II. Ce-$4f$ electron occupancy, n_f, and probabilities of $4f^0$, $4f^1$, and f^2 for Ce1 in the DFT+DMFT calculations.

n_f (electron/Ce atom)	Ce1	Ce2	P($4f^0$)	P($4f^1$)	P($4f^2$)
$CeCoIn_5$	1.0432	1.0432	0.0341	0.9126	0.0532
$CeCo(In_{0.9}Cd_{0.1})_5$	1.0299	1.0329	0.0297	0.9267	0.0434
$CeCo(In_{0.9}Hg_{0.1})_5$	1.0214	1.0362	0.028	0.9224	0.0495
$CeCo(In_{0.9}Sn_{0.1})_5$	1.0822	1.0452	0.064	0.8711	0.0646

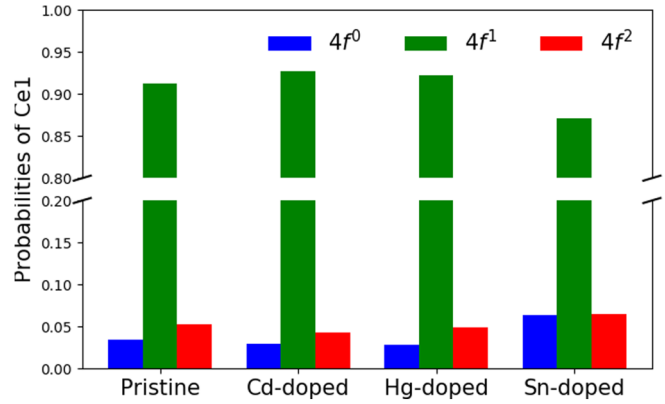

FIG. 4. The calculated probabilities of valence states for $n_f = 0$ (blue), 1 (green), and 2 (red) of Ce1 in the pristine and doped cases.

simultaneously the probabilities of f^0 and f^2 configurations increase. We thus conclude that the calculated n_f measures both the Ce-$4f$ electron count for both low-energy and high-energy configuration states. The overall differences of n_f are less than 0.1 electron per Ce atom. However, the correlation effect enables the fine-tuned electron number to bring up the drastic change of its electronic structure.

We investigate the calculated hybridization function ($-\mathrm{Im}\Delta$) for Ce1 and Ce2, as shown in Figs. 5(a) and 5(b). Compared to Figs. 2(a) and 2(b), the DFT+DMFT calculation shows that the hybridization strength increases with the number of valence electrons. In energy between

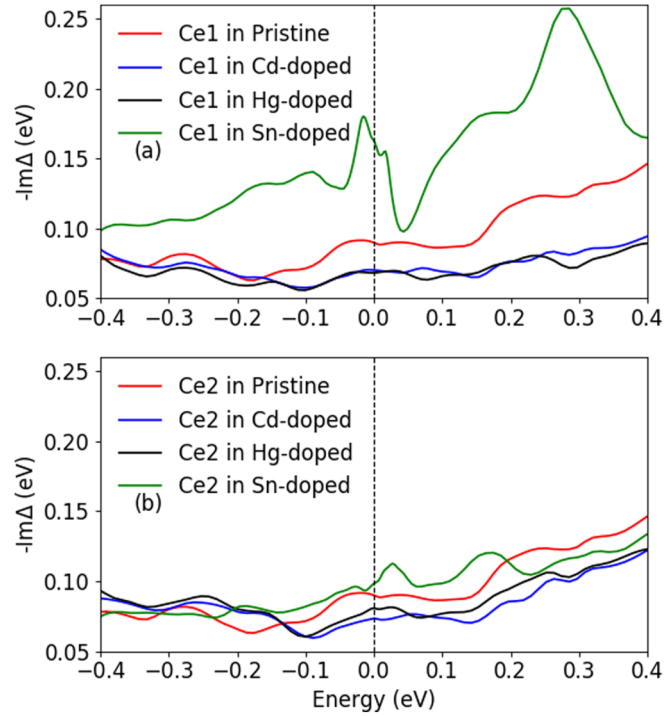

FIG. 5. The imaginary part of the hybridization functions for (a) Ce1 $j = 5/2$ states and (b) Ce2 $j = 5/2$ states in different structures with DFT+DMFT. The labels represent $CeCoIn_5$ (pristine), $CeCo(In_{0.9}Cd_{0.1})_5$, $CeCo(In_{0.9}Hg_{0.1})_5$, and $CeCo(In_{0.9}Sn_{0.1})_5$.

TABLE III. Summary of the hybridization strength $-\mathrm{Im}\Delta(0)$.

$-\mathrm{Im}\Delta(0)$ (eV)	Ce1 $j = 5/2$ states	Ce2 $j = 5/2$ states
$CeCoIn_5$	0.08999	0.08999
$CeCo(In_{0.9}Cd_{0.1})_5$	0.07032	0.07345
$CeCo(In_{0.9}Hg_{0.1})_5$	0.06837	0.08064
$CeCo(In_{0.9}Sn_{0.1})_5$	0.16292	0.0982

-0.1 and 0.1 eV, the dopant-dependent hybridization functions are well illustrated with respect to the red lines (pristine). The imaginary part of the hybridization $[-\mathrm{Im}\Delta(\omega = 0)]$ at E_F of Ce1 in Sn-doped $CeCoIn_5$ is enhanced significantly over the other cases (see Table III). This enhancement of hybridization is reduced to be comparable to the pristine case for Ce2. This could be understood in terms of the relative distances between the Ce atoms and the Sn atom. The substitution of a hole (Cd, Hg) decreases $-\mathrm{Im}\Delta(\omega = 0)$ around E_F. Both Cd and Hg dopants give rise to similar decreases of the $-\mathrm{Im}\Delta(\omega = 0)$ on both Ce1 and Ce2 with respect to the pristine cases. The behavior shown in $-\mathrm{Im}\Delta$ and $-\mathrm{ImG_{loc}}$ could reveal how the hybridization is changed in each case. The reduction of the hybridization favors a local-moment ground state over the Fermi-liquid phase. We conclude that Sn-doped (Cd- or Hg-doped) $CeCoIn_5$ would be in proximity to a Fermi-liquid state (a magnetic ground state).

To elaborate more insight into the renormalization of the quasiparticle state, we will examine the imaginary (Im) and real (Re) parts of the calculated self-energy (Σ). Here the

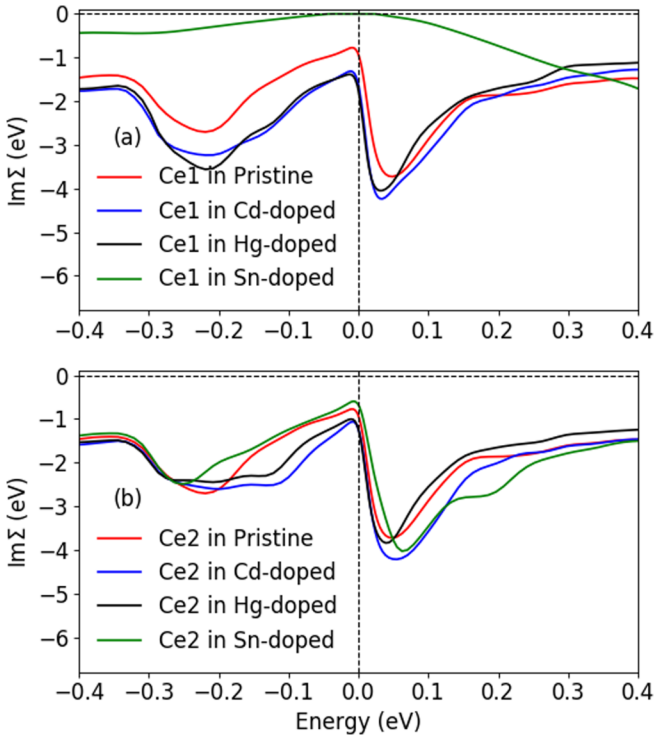

FIG. 6. The imaginary part of the self-energy for (a) Ce1 $j = 5/2$ states and (b) Ce2 $j = 5/2$ states in different structures with DFT+DMFT. The labels represent $CeCoIn_5$ (pristine), $CeCo(In_{0.9}Cd_{0.1})_5$, $CeCo(In_{0.9}Hg_{0.1})_5$, and $CeCo(In_{0.9}Sn_{0.1})_5$.

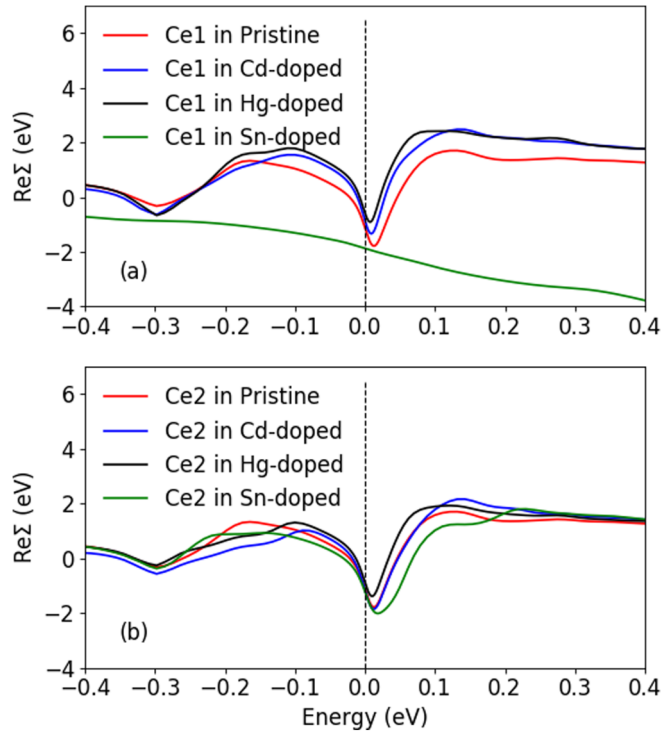

FIG. 7. The real part of the self-energy for (a) Ce1 $j = 5/2$ states and (b) Ce2 $j = 5/2$ states in different structures with DFT+DMFT. The labels represent $CeCoIn_5$ (pristine), $CeCo(In_{0.9}Cd_{0.1})_5$, $CeCo(In_{0.9}Hg_{0.1})_5$, and $CeCo(In_{0.9}Sn_{0.1})_5$.

Green's functions are retarded ones, which ensures a negative imaginary part of the self-energies. Figure 6 shows the imaginary part of the self-energy ($\mathrm{Im}\Sigma$), whose inverse at E_F represents the inverse of the lifetime of the quasiparticle state. $\mathrm{Im}\Sigma(\omega = 0)$ of Ce1 in the Sn-doped case is almost zero at $T = 0.005$ eV ($\sim$65 K). The parabolic behavior of $\mathrm{Im}\Sigma$ around $\omega = 0$ of Ce1 in Sn-doped $CeCoIn_5$ is a typical Fermi-liquid characteristic. The Fermi-liquid phase represents the presence of the coherent quasiparticle states. The finite values of $\mathrm{Im}\Sigma$ ($\omega = 0$) indicate the deviation from the Fermi-liquid phase in the other cases. This quasiparticle state of the Ce1 in $CeCo(In_{0.9}Sn_{0.1})_5$ would be consistent with the largely enhanced hybridization function.

The renormalization of the band is strongly associated with the mass enhancement under correlation. The slope of $\mathrm{Re}\Sigma$ at E_F is used to represent how a large correlation effect reduces the bandwidth of a quasiparticle state. Figure 7 provides the variation of $\mathrm{Re}\Sigma$ from -0.4 to 0.4 eV. The slopes of $\mathrm{Re}\Sigma$ at E_F seem to be similar to the red lines of the pristine case,

TABLE IV. Summary of the quasiparticle weight (Z) at the Fermi energy E_F.

$Z\ [1/(1 - \frac{\partial \mathrm{Re}\Sigma}{\partial \omega})$ at $E_F]$	Ce1 $j = 5/2$ states	Ce2 $j = 5/2$ states
$CeCoIn_5$	0.0124	0.0124
$CeCo(In_{0.9}Cd_{0.1})_5$	0.0110	0.0110
$CeCo(In_{0.9}Hg_{0.1})_5$	0.0121	0.0121
$CeCo(In_{0.9}Sn_{0.1})_5$	0.1100	0.0139

TABLE V. Calculation of Kondo temperature, $T_{\mathrm{Kondo}} = -\pi Z \mathrm{Im}\Delta(0)/4$.

T_{Kondo} (eV)	Ce1 $j = 5/2$ states	Ce2 $j = 5/2$ states
$CeCoIn_5$	0.00087	0.00087
$CeCo(In_{0.9}Cd_{0.1})_5$	0.000607	0.000634
$CeCo(In_{0.9}Hg_{0.1})_5$	0.000649	0.000766
$CeCo(In_{0.9}Sn_{0.1})_5$	0.0140	0.001071

except for that of Ce1 in the Sn-doped case. The quasiparticle weight Z is computed using $1/(1 - \frac{\partial \mathrm{Re}\Sigma}{\partial \omega})$ at E_F and is given in Table IV. The $\mathrm{Re}\Sigma(\omega = 0)$ of the Ce1 shows a very different behavior in comparison to the other cases. More strikingly, the quasiparticle weight Z (0.11) of the Ce1 in the Sn-doped $CeCoIn_5$ is nearly one order of magnitude larger than that for both the pristine and hole-doped cases. The larger quasiparticle weight represents the larger overlap of the correlate and noninteracting wave function at E_F. The weight for the Ce2 is around 0.0139, which is slightly larger than the other cases [see Fig. 7(b)]. The inhomogeneity due to the Sn dopant is consistently observed in the DFT+DMFT calculations. On the other hand, the quasiparticle weight for the hole-doped $CeCoIn_5$ is 0.011 (Cd-doped) and 0.012 (Hg-doped), respectively. This is also consistent with the observation that the bandwidths of the pristine and the hole-doped $CeCoIn_5$ compounds are similarly renormalized [see Fig. 3(a)]. The inhomogeneity due to the hole dopant is relatively suppressed in the DFT+DMFT calculations.

Using the calculated Z and $\mathrm{Im}\Delta$, the Kondo temperature (T_{Kondo}) could be predicted with the empirical formula $T_{Kondo} = -\pi Z \mathrm{Im}\Delta(0)/4$ [39]. T_{Kondo} represents $4f$ electrons undergoing a renormalized Fermi-liquid phase with the highly enhanced effective mass. The calculated T_{Kondo} is summarized in Table V. The largest T_{Kondo} is 0.0140 eV for Ce1 in $CeCo(In_{0.9}Sn_{0.1})_5$, which is one order of magnitude larger than the used temperature ($T = 0.005$ eV). However, The T_{Kondo} for Ce2 in $CeCo(In_{0.9}Sn_{0.1})_5$ is reduced to 0.001 071 eV, which is still higher than all other Kondo temperatures in the hole-doped compounds. These results suggest the substantial enhancement effect of the Sn dopant on the Kondo coherence, which pushes the system to be closer to the Fermi-liquid phase, and a robust nonequivalence of the Kondo coherence between Ce1 and Ce2 through the DFT+DMFT iterations. The hole-doped case shows the decrease in both the $-\mathrm{Im}\Delta$ and Z at E_F. Therefore, T_{Kondo} in the hole-doped cases is lower than those of the pristine case. Unlike the electron-doped case, Ce1 and Ce2 simultaneously become more incoherent at $T = 0.005$ eV.

IV. CONCLUDING REMARKS AND SUMMARY

Since dopants prefer to be substituted in the Ce plane [13], our study here has considered the spatial inhomogeneity in the doped $CeCoIn_5$ system. The much enhanced hybridization Δ and the non-Ce-$4f$ density of states N_F of Ce1 near Sn can drive the system deep into the Fermi-liquid state. We have also found through the two single-site DMFT impurity solvers that the $4f$-electron behavior is dramatically different on Ce1 and Ce2. Furthermore, the current study has shown a short-range electron doping effect. On the contrary, in the case of hole-doped $CeCoIn_5$, the Ce-$4f$ state would be more incoherent than in the pristine state. We further note that our study has been limited to the paramagnetic solutions and, as such, the presence of a G-type antiferromagnetic configuration [$q = (\pi, \pi, \pi)$], as reported in the Cd-doped $CeCoIn_5$ [10], is beyond the scope of the present work. However, the dopant-induced incoherence obtained here, indicating that the state moves away from the Fermi-liquid phase, is consistent with the experiment. It is worthwhile to note that while the Sn doping gives a stronger inhomogeneity effect on the local electronic structure, the NMR experiment has observed [24] that the Cd doping causes a stronger inhomogeneity effect on the magnetic fluctuations.

In summary, we have investigated the inhomogeneous hole and electron doping effect on $CeCoIn_5$ within the DFT+DMFT framework. We have revealed a clear variation of the hybridization function as well as the highly renormalized bands of Ce-$4f$ states. In addition, the calculated T_{Kondo} has provided a good insight into whether Ce-$4f$ states in a doped $CeCoIn_5$ system would be coherent or incoherent. Specifically, we have discovered a highly inhomogeneous influence of Sn substitution on Ce-$4f$ electron states. This prediction should be accessible to scanning tunneling microscopy experiments on a (100)- or (010)-oriented surface of a Sn-doped $CeCoIn_5$.

ACKNOWLEDGMENTS

H.C.C. thanks Soobeom Seo for illuminating discussions. This work was carried out under the auspices of the U.S. Department of Energy (DOE) National Nuclear Security Administration (NNSA) under Contract No. 89233218CNA000001. It was supported by the LANL LDRD Program (H.C.C.), the DOE BES "Quantum Fluctuations in Narrow Band Systems" project (E.D.B., F.R.), and the NNSA Advanced Simulation and Computing Program (J.-X.Z.). Additional support has been provided in part by the Center for Integrated Nanotechnologies, a DOE BES user facility, in partnership with the LANL Institutional Computing Program for computational resources. H.C.C. was also supported by the Institute for Basic Science in Korea (Grant No. IBS-R009-D1).

[1] P. Fulde, *Electron Correlations in Molecules and Solids* (Springer, Berlin, 1995).

[2] P. Fulde, P. Thalmeier, and G. Zwicknagl, *Solid State Physics*, Vol. 60 (Academic, New York, 2006).

[3] C. Pfleiderer, Rev. Mod. Phys. **81**, 1551 (2009).

[4] N. Mathur, F. Grosche, S. Julian, I. Walker, D. Freye, R. Haselwimmer, and G. Lonzarich, Nature (London) **394**, 39 (1998).

[5] G. Knebel, D. Braithwaite, P. C. Canfield, G. Lapertot, and J. Flouquet, Phys. Rev. B **65**, 024425 (2001).

[6] C. Petrovic, P. Pagliuso, M. Hundley, R. Movshovich, J. Sarrao, J. Thompson, Z. Fisk, and P. Monthoux, J. Phys.: Condens. Matter **13**, L337 (2001).
[7] H. Hegger, C. Petrovic, E. G. Moshopoulou, M. F. Hundley, J. L. Sarrao, Z. Fisk, and J. D. Thompson, Phys. Rev. Lett. **84**, 4986 (2000).
[8] C. Petrovic, R. Movshovich, M. Jaime, P. Pagliuso, M. Hundley, J. Sarrao, Z. Fisk, and J. Thompson, Europhs. Lett. **53**, 354 (2001).
[9] L. D. Pham, T. Park, S. Maquilon, J. D. Thompson, and Z. Fisk, Phys. Rev. Lett. **97**, 056404 (2006).
[10] M. Nicklas, O. Stockert, T. Park, K. Habicht, K. Kiefer, L. D. Pham, J. D. Thompson, Z. Fisk, and F. Steglich, Phys. Rev. B **76**, 052401 (2007).
[11] R. R. Urbano, B.-L. Young, N. J. Curro, J. D. Thompson, L. D. Pham, and Z. Fisk, Phys. Rev. Lett. **99**, 146402 (2007).
[12] J. Rusz, P. M. Oppeneer, N. J. Curro, R. R. Urbano, B.-L. Young, S. Lebégue, P. G. Pagliuso, L. D. Pham, E. D. Bauer, J. L. Sarrao, and Z. Fisk, Phys. Rev. B **77**, 245124 (2008).
[13] C. H. Booth, E. D. Bauer, A. D. Bianchi, F. Ronning, J. D. Thompson, J. L. Sarrao, J. Y. Cho, J. Y. Chan, C. Capan, and Z. Fisk, Phys. Rev. B **79**, 144519 (2009).
[14] K. Gofryk, F. Ronning, J.-X. Zhu, M. N. Ou, P. H. Tobash, S. S. Stoyko, X. Lu, A. Mar, T. Park, E. D. Bauer, J. D. Thompson, and Z. Fisk, Phys. Rev. Lett. **109**, 186402 (2012).
[15] H. Sakai, F. Ronning, T. Hattori, Y. Tokunaga, S. Kambe, J.-X. Zhu, N. Wakeham, H. Yasuoka, E. D. Bauer, and J. D. Thompson, J. Phys.: Conf. Ser. **807**, 032001 (2017).
[16] Q. Y. Chen, F. Ronning, E. D. Bauer, C. H. P. Wen, Y. B. Huang, and D. L. Feng, Phys. Rev. B **100**, 235148 (2019).
[17] M. N. Ou, K. Gofryk, R. E. Baumbach, S. S. Stoyko, J. D. Thompson, J. M. Lawrence, E. D. Bauer, F. Ronning, A. Mar, and Y. Y. Chen, Phys. Rev. B **88**, 195134 (2013).
[18] E. D. Bauer, C. Capan, F. Ronning, R. Movshovich, J. D. Thompson, and J. L. Sarrao, Phys. Rev. Lett. **94**, 047001 (2005).
[19] E. Bauer, N. Moreno, D. Mixson, J. L. Sarrao, J. Thompson, M. F. Hundley, R. Movshovich, and P. Pagliuso, Phys. B: Condens. Matter **359**, 35 (2005).
[20] E. D. Bauer, F. Ronning, C. Capan, M. J. Graf, D. Vandervelde, H. Q. Yuan, M. B. Salamon, D. J. Mixson, N. O. Moreno, S. Brown, J. D. Thompson, R. Movshovich, M. F. Hundley, J. L. Sarrao, P. G. Pagliuso, and S. M. Kauzlarich, Phys. Rev. B **73**, 245109 (2006).
[21] M. Daniel, E. D. Bauer, S.-W. Han, C. H. Booth, A. L. Cornelius, P. G. Pagliuso, and J. L. Sarrao, Phys. Rev. Lett. **95**, 016406 (2005).
[22] M. Yokoyama, K. Fujimura, S. Ishikawa, M. Kimura, T. Hasegawa, I. Kawasaki, K. Tenya, Y. Kono, and T. Sakakibara, J. Phys. Soc. Jpn. **83**, 033706 (2014).
[23] T. B. Park, S. Shin, S. Lee, S. Seo, H. Jang, J. Kim, H. Lee, H. Wang, H. Lee, and T. Park, Phys. Rev. Materials **4**, 084801 (2020).
[24] H. Sakai, F. Ronning, J.-X. Zhu, N. Wakeham, H. Yasuoka, Y. Tokunaga, S. Kambe, E. D. Bauer, and J. D. Thompson, Phys. Rev. B **92**, 121105(R) (2015).
[25] J. Shim, K. Haule, and G. Kotliar, Science **318**, 1615 (2007).
[26] H. C. Choi, B. I. Min, J. H. Shim, K. Haule, and G. Kotliar, Phys. Rev. Lett. **108**, 016402 (2012).
[27] T. Nomoto and H. Ikeda, Phys. Rev. B **90**, 125147 (2014).
[28] S. Seo, E. Park, E. Bauer, F. Ronning, J. Kim, J.-H. Shim, J. Thompson, and T. Park, Nat. Commun. **6**, 6433 (2015).
[29] G. Kotliar, S. Y. Savrasov, K. Haule, V. S. Oudovenko, O. Parcollet, and C. A. Marianetti, Rev. Mod. Phys. **78**, 865 (2006).
[30] K. Haule, C.-H. Yee, and K. Kim, Phys. Rev. B **81**, 195107 (2010).
[31] P. Blaha, K. Schwarz, G. K. H. Madsen, D. Kvasnicka, and J. Luitz Schwarz, *WIEN2K an Augmented Plane Wave Local Orbitals Program for Calculating Crystal Properties* (Vienna University of Technology, Vienna, 2001).
[32] T. Pruschke and N. Grewe, Z. Phys. B **74**, 439 (1989).
[33] K. Haule, S. Kirchner, J. Kroha, and P. Wölfle, Phys. Rev. B **64**, 155111 (2001).
[34] S. Schmitt, T. Jabben, and N. Grewe, Phys. Rev. B **80**, 235130 (2009).
[35] R. D. Cowan, *The Theory of Atomic Structure and Spectra*, Vol. 3 (University of California Press, Berkeley, 1981).
[36] B. G. Jang, B. Goh, J. N. Kim, H. Kang, J. H. Shim, H. Choi, K. Haule, and G. Kotliar, arXiv:2007.10641.
[37] K. Momma and F. Izumi, J. Appl. Crystallogr. **44**, 1272 (2011).
[38] N. E. Bickers, D. L. Cox, and J. W. Wilkins, Phys. Rev. B **36**, 2036 (1987).
[39] J.-X. Zhu, R. C. Albers, K. Haule, and J. M. Wills, Phys. Rev. B **91**, 165126 (2015).